Detection of Micron-Sized Chemical Droplets Using a Commodity Digital Camera Setup

Hongli Jiang, S. Hessam M. Mehr*
School of Chemistry, the University of Glasgow, University Avenue, Glasgow G12 8QQ, UK.

Abstract

The availability, portability, and low cost of electronic devices have made them a prime candidate for the rapid detection of chemical particles. Here we designed a chemical particle detection system based on a Raspberry Pi camera to detect micron droplets generated by ultrasonic atomizers. Through the analysis of sample photos and droplet size, we found that the detection system could clearly image micron-sized particles and accurately measure the particle size. The devices used in this system were all low-cost widely accessible digital cameras, so this detection technique could meet the requirements of low-cost and rapid detection technology, and widely deployed as a practical readout method in chemistry experiments.

Background

The detection of chemical particles is of great practical importance, like detection of indoor air safety in daily life,[1,2] and detection of engineered particles in industrial field (3), and detection of biological macromolecules in scientific research (4).

The above three cases are representatives of the importance of detecting chemical particles. In modern life, there are much more applications that need the detection of chemical particles. Therefore, it is necessary to find and develop suitable chemical particle detection techniques.

Common particle detection and imaging techniques include optical microscope with super high resolution, Transmission Electron Microscope (TEM), Scanning Electron Microscope (SEM), and Atomic Force Microscope (AFM). Although the large-scale imaging instruments such as TEM, SEM and AFM can image nanoparticles clearly, they are expensive, bulky, and nanoscale imaging, which is overqualified for daily rapid detection of chemical particles (5), so this kind of instruments are not suitable for large-scale popular use. Historically commodity digital cameras have been cheaper but weren't applicable, but now there are better sensors and lenses available. The availability, portability, and low cost of this kind of electronic devices have made them one of the research hotspots for the rapid detection of chemical particles.

The principle of particle detection technology based on commodity digital cameras is similar to that of optical microscopes, and the imaging performance is related to the light-absorbing properties of the detected objects. For those substances that do not absorb visible light or UV light, the detected object first needs to be processed to be given light-absorbing properties, such

*Email: Hessam.Mehr@glasgow.ac.uk

as being introduced light absorbing or fluorescent groups in molecular structures, or being combined with light absorbing or fluorescent substances, and then the objects can be detected by detection system based on commodity digital cameras. Below we showcase successful applications of commodity smartphone cameras to the detection and characterisation of microscopic chemical and biological objects.

This paper was informed by some prior work of detection of chemical particles as follows:

To detect the Schistosoma which absorbs visible light, Isaac I. Bogoch et al. (6) designed a smartphone-based detection system which can detect particle diameter as small as 0.87μm. The basic structure of the system consisted with a smartphone and an external lens, which indicated this paper that with the help of external lens, micron-sized particles could be easily detected.

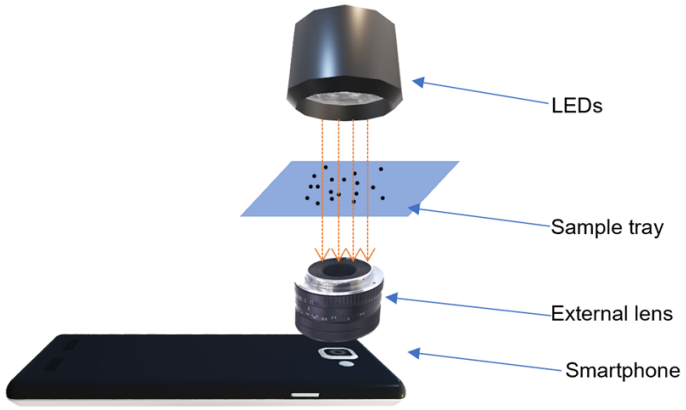

Figure 1. The schematic demonstrating the design of the microscope system in Isaac I. Bogoch's experiment.

To detect fluorescent particles that absorbs UV light, Wei (7) et al. designed a similar smartphone-based detection system, but they added a laser diode to act as a fluorescence exciter. Wei's study showed that the smartphone-based detection system combined with a fluorescence exciter can observe micron-sized fluorescent particles well.

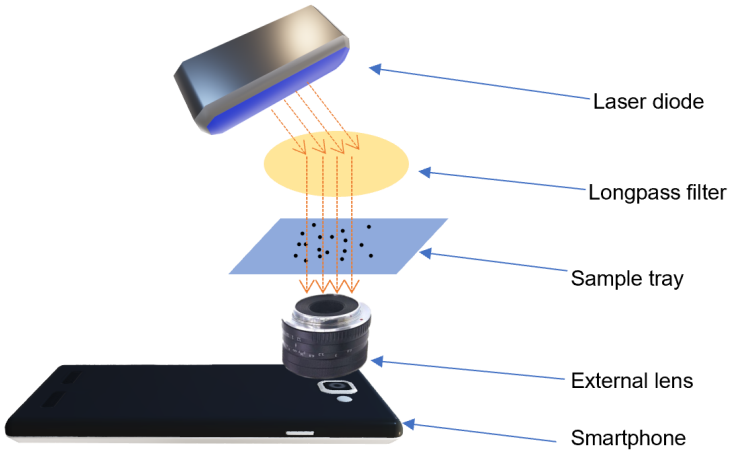

Figure 2. The schematic of Wei's imaging system.

To detect viruses that do not absorb visible or UV light, Zeying et al. (8) designed a printed dielectric nanochain assay, which gave this paper a good idea to detect the third kind of particles. To solve the unobservability of this kind particles, Zeying combined specific viruses and observed nanochains through specific antibodies embedded on the surface of the nanochains, which allowed the combination to be detected.

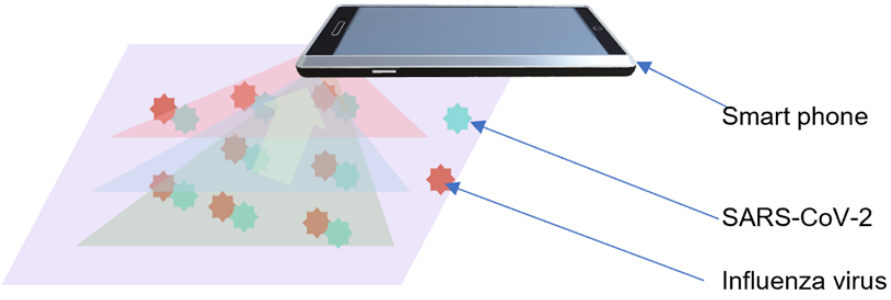

Figure 3. The principle of Zeying's detection system (8).

In conclusion, a series of studies have shown that detection systems based on commodity digital cameras can accurately detect chemical particles at the micron or even nanometre scale, and it is also a fast, efficient and low-cost method for chemical particle detection. In addition, most of the current research on commodity digital cameras microscope imaging systems focuses on the situation where the sample to be detected is in solution, while in real life there are many scenarios that require direct detection of solid surfaces, such as rapid detection of coronavirus on floors, door handles, etc. Therefore, more research is needed to focus on how to directly detect the chemical particles on the solid surface, or how to transfer the particles on the solid surface to the solution or test paper for accurate detection.

Materials and Methods

Considering the microscopic imaging system based on commodity digital cameras and the questions raised before, this project used micron-scale droplets to simulate chemical particles, and then combined a Raspberry Pi camera with a Zoom-stereomicroscope to detect the micron-scale droplets on solid surfaces, including the size, colour, and coordinates of the droplets. The project was divided into four phases:

Phase I: Sample preparation, including single colour and complex colour sample preparation for visible-light-absorbing substances and sample preparation for fluorescent substances.

Phase II: Photographing and detection of visible-light-absorbing samples.

Phase III: Photographing and detection of fluorescent samples.

Phase IV: Accuracy validation of the designed detection system.

Non-fluorescent and fluorescent dyes. Most particle detections are based on visible or UV light

absorption. For those substances that do not absorb the two kinds of light, the analyte can be pre-treated to have the absorption properties. Therefore, two kinds of samples were designed in this project, visible-light-absorbing samples and fluorescent samples.

For the selection of visible-light-absorbing substances, this project designed two kinds of samples, a single-colour sample and a complex-colour sample. The single-colour sample was made of blue ink, which is Bleu Pervenche fountain pen ink. However, in scientific research or daily life, the samples to be tested are usually composed of multi-component or multi-coloured particles, so this project designed the complex-colour sample, which is composed of blue ink droplets and Rose Bengal droplets.

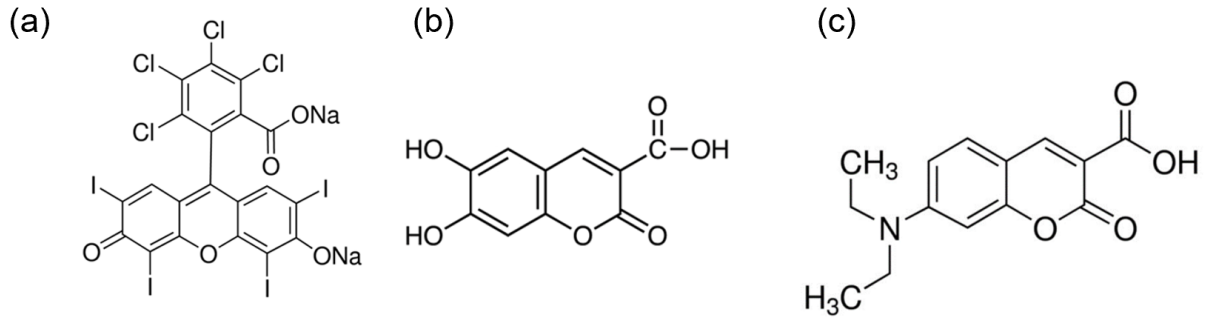

Figure 4. Molecular structure of dyes used in droplet formulations. (a) Rose bengal; (b) 6,7-dihydroxycoumarin-3-carboxylic acid; (c) 7-(diethylamino)-coumarin-3-carboxylic acid.

For the selection of fluorescent substances, initially a randomly selection one of fluorescent dyes was used for sample preparation. However, initial experiments suggested that it was found that the fluorescent dye can only be excited by UV light in the dilute solution state, due to fluorescence quenching in the absence of solvent. This phenomenon occurs because in the solid state, strong π-π stacking of aromatic rings adjacent to the fluorophore results in ordered or disordered aggregates that do not emit radiation when they decay from excited states, which means they do not produce fluorescence, also known as aggregation-caused quenching (ACQ) (12).

Figure 5. Image showing the chemical mechanism of ACQ and AIE (12)

However, Jingdong Luo et al. (13) found that some fluorescent dyes can still emit strong

fluorescence in the solid state, which is called the Aggregation-induced emission (AIE) effect. Therefore, this project selected two dyes that have AIE effect, 6,7-Dihydroxycoumarin-3-carboxylic acid and 7-(Diethylamino)-coumarin-3-carboxylic acid.

Experimentation

Sampling system. The sampling system used in this system included: ultrasonic atomizer × 1, iron stand × 1, three-claw clip × 2, glass slide × 2 and ruler × 1.

As the picture below shows, the ultrasonic atomizer was fixed on glass slide G1 located on the base of the iron frame, and another glass slide G2 fixed by a three-claw clip C1 was used to collect the droplets, and above the glass slide G2, there was another three-claw clip C2 used to fix the rule, which was used for measuring the sampling height. After testing, it was proved that the suitable distance between the G1 (ultrasonic atomizer) and the G2 was 8cm (sampling height).

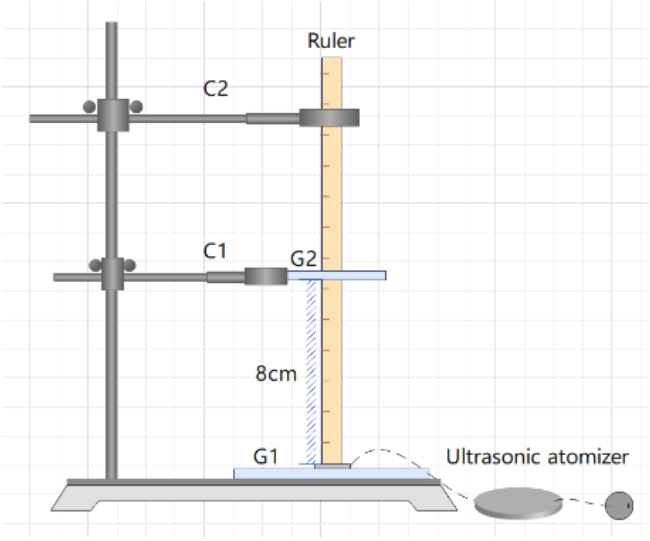

Figure 6. Schematic diagram of the sampling system.

The blue ink was used as the raw material to prepare samples for testing the feasibility of the sampling system.

During the experiment, 3 drops of blue ink were added on the surface of the atomizer, and the switch of the atomizer was turned on at the same time. After 5 seconds, it could be clearly seen that blue vapor was produced and went upward from the micro-hole of the atomizer. After 20 seconds, the surface of the glass slide became light blue, which means the sampling was finished.

Then the glass slide was observed with the high-resolution microscope, and it was clearly seen that the surface of the glass slide was covered with blue circular spots, and the diameter of a spot is 28.83 microns, which proved the feasibility of the sampling system.

Sample preparation

The visible-light-absorbing substances used in this project were blue ink and Rose Bengal dye.

After testing, the suitable formulations of the two solutions are shown in the Table 1.

Solution	Solute	Solvent
Blue ink	Original concentration	
Rose Bengal Aqueous Solution	37mg	5ml Water

Table 1. Solution formulations of visible-light-absorbing samples.

The preparation method of the single-colour sample (blue droplet sample) was the same as before, and the complex-colour sample was made as follows.

a. A blue ink sample was first prepared according to the method mentioned before (sampling height is 8cm, sampling time is 25s).
b. The glass slide G2 and the atomizer were then cleaned, and 3 drops of Rose Bengal aqueous solution were dropped on the atomizer, the step a was repeated and the collection of the second droplets was then finished.

As mentioned before, this project required dyes that could be excited by UV light in the solid state, so 7-(Diethylamino)-coumarin-3-carboxylic acid and 6,7-Dihydroxycoumarin-3-carboxylic acid were selected. The two dyes are both soluble in organic solvents, so Dimethylformamide (DMF) which is common in the laboratory was selected as the solvent in this project. After testing, the suitable solution formula is as follows:

Solution	Solute	Solvent
7-(Diethylamino)-coumarin-3-carboxylic acid solution	20mg	2ml DMF
6,7-Dihydroxycoumarin-3-carboxylic acid solution	20mg	2ml DMF

Table 2. Solution formulations of fluorescent samples.

The sample preparation method was similar to before, the sampling devices and sampling height were the same, but the difference was the sampling time, which was due to the different properties (viscosity and surface tension) of the organic solvent DMF and water.

The viscosity of DMF is 0.802 mPa·s and the surface tension is 25.7 dyne/cm, while the viscosity of water is 2.98 mPa·s and the surface tension is 72.8 mN/m. According to the research of C.E.Ejim et al. (15), when other conditions remained the same, the size of liquid atomized particles would increase with the increase of viscosity or surface tension. Therefore, when the atomizer was powered on, the atomized particles generated by DMF liquid were much smaller than those generated by water, so at the initial stage of atomization, the DMF atomized particles would be too small to be observed by naked eyes until a period, which was longer than the time required for water atomization. After testing, the project determined that the DMF solution sampling time was approximately 50 seconds.

Photographing of samples

For the non-fluorescent sample:

a. The camera system was assembled according to the requirements mentioned before.
b. The intensity and magnification of the Zoom-stereomicroscope were adjusted. (For the convenience of subsequent image processing and size measurement, the zoom-in value was set to 3.2).
c. The photographing program was run to complete the photographing of the sample.

The photographing process of fluorescent samples was similar to that of visible-light-absorbing samples. It was worth noting that due to the droplets with small size in the fluorescent samples, the intensity of fluorescence spots was weak, so it was necessary to adjust the frame rate and shutter speed of photographing in the photographing program to achieve clear capture of fluorescence spots.

Determination of image scale

After the sample photos was obtained, the Python code was needed to detect droplet size and position, but the detection results of the Python work showed the pixel size of the droplets. Meanwhile, because every sample photo was a part of the glass slide, it could not be determined according to the known information. Therefore, to determine the actual size of the droplets, the scale of the image needed to be measured.

The method used in this project are as follows:

a. Pick a rule with a minimum scale value of 0.5mm.
b. Take a picture of this ruler according to the photographing method (zoom-in value is 3.2).
c. After taking the photo, draw two parallel lines along the tick marks, and then make another line perpendicular to the two parallel lines. The three lines will produce two intersections, point A and point B of which the real distance is 0.5mm.
d. Use Python to measure the pixel difference between the two points A and B, and the pixel difference corresponds to 0.5mm, according to which the scale of the image under the microscope zoom-in value of 3.2 can be determined.

Results and Discussion

Droplet size

The test sample was prepared according to the sampling method described before, and its observation result with the high-resolution microscope are shown in the figure below.

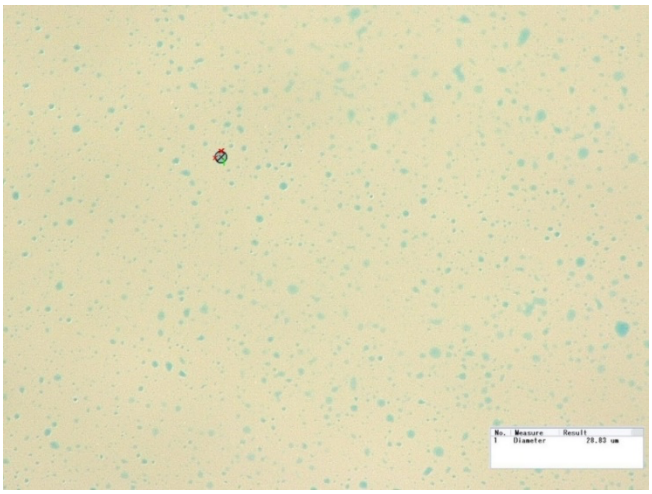

Figure 7. Picture of the test sample taken by the camera system, showing the droplet size is at micron level.

It could be clearly seen from the picture that there were many blue circular spots distributed on the surface of the glass slide, and one spot was marked with a black circle whose diameter was 28.83 μm. This proved that the sampling system designed in this project was feasible, which meant the collected droplets were at the micron level. Meanwhile, it was worth noting there were many blue spots with diameter much smaller than 28.83 μm in the sample, and the size of these spots reached the sub-micron level. Therefore, the droplets prepared by the sampling system could accurately simulate most common chemical particles.

Image scale

When the microscope zoom-in value was set to 3.2, the picture of a ruler with a minimum scale of 0.5mm was as shown in the figure below.

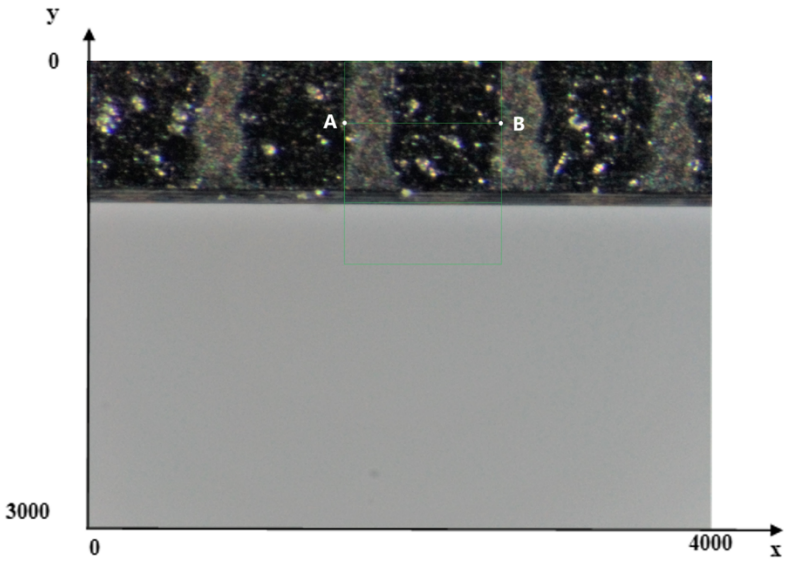

Figure 8. Picture of the ruler divisions marks taken by the camera system and used to calibrate

the length scale.

The real distance between point A and point B is 0.5mm. After Python work of this image, the coordinates of the two points were determined: A (1670,400), B (2690,400). Therefore, the pixel difference between points A and B was 1020 pixels, which meant that when the zoom-in value was 3.2, the real size corresponding to one pixel is 0.5mm/1020≈0.5μm/pixel.

Photographing and detection of visible-light-absorbing samples

Single-colour sample

The photo of the single-colour sample and detection of the single-colour droplets using OpenCV is shown in Figure 9.

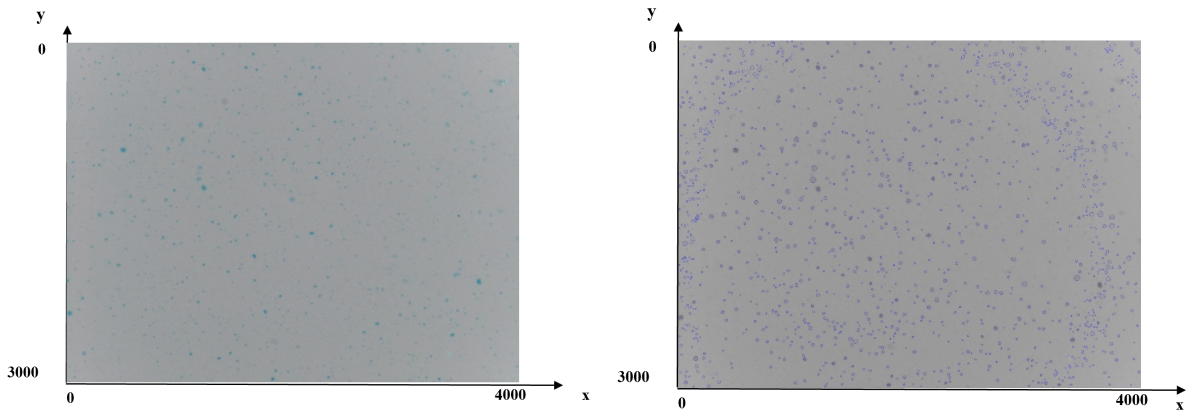

Figure 9. Single-colour sample imaged using the camera system (left) and detected droplets using OpenCV (right).

The sampling performance of this sample was similar to that of the test sample: most of the blobs were regular circles with uniform location distribution, which was beneficial for subsequent image processing.

The detection results showed that the area of the observation area was 3mm², and there were a total of 1327 droplets. The average diameter of these droplets was 9.44μm and the average area was 79.04μm².

	Droplet of largest size	Droplet of smallest size
Pixel coordinates	（3495, 2076）	（3452, 2954）
Diameter(μm)	24.87	4.89
Area(μm²)	485.82	18.83

Table 3. Data for the largest and smallest droplets in the simple-colour sample.

The diameter distribution of blobs is shown in Figure 10.

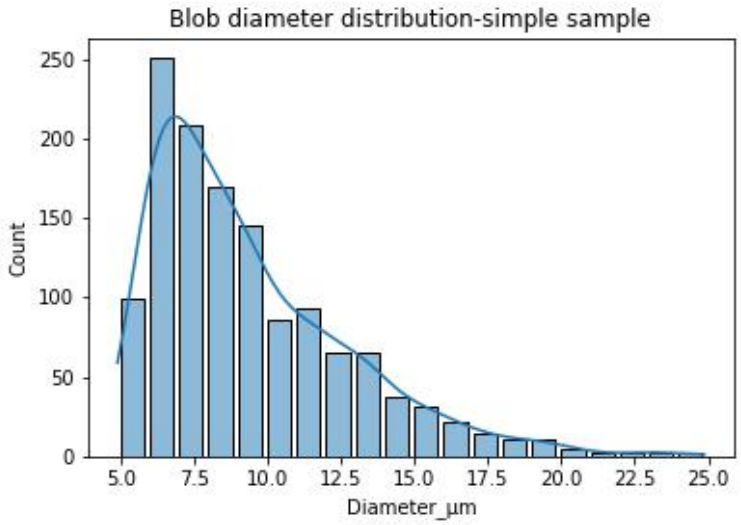

Figure 10. Diameter distribution of the simple-colour sample.

It is shown from the above figure that the largest distribution of blob diameters in the detection area was 5.90 μm–6.90 μm, accounting for 18.91% of the quantity. The diameters of most of the blobs ranged from 4.90 μm to 14.90 μm, and the quantity accounted for 84.33%.

Droplet concentration	Value
Droplet area concentration (%) Total droplet area / detection area	$1327 \times 79.04 \div 3 \times 10^6 = 3.49\%$
Quantity concentration (particles/mm²) Quantity of droplets / detection area	$1327 \div 3 = 442$

Table 4. Droplet concentration of the simple-colour sample.

Therefore, in the simple-colour sample, the number of the droplets was 1327. The diameter range of droplets was from 4.89 to 24.87μm. 84.33% of droplets were at the range of 4.90 μm to 14.90 μm. The area concentration and quantity concentration of the droplets were 3.49% and 442 / mm² respectively.

Complex-colour sample

The photograph of the complex colour sample is as follows:

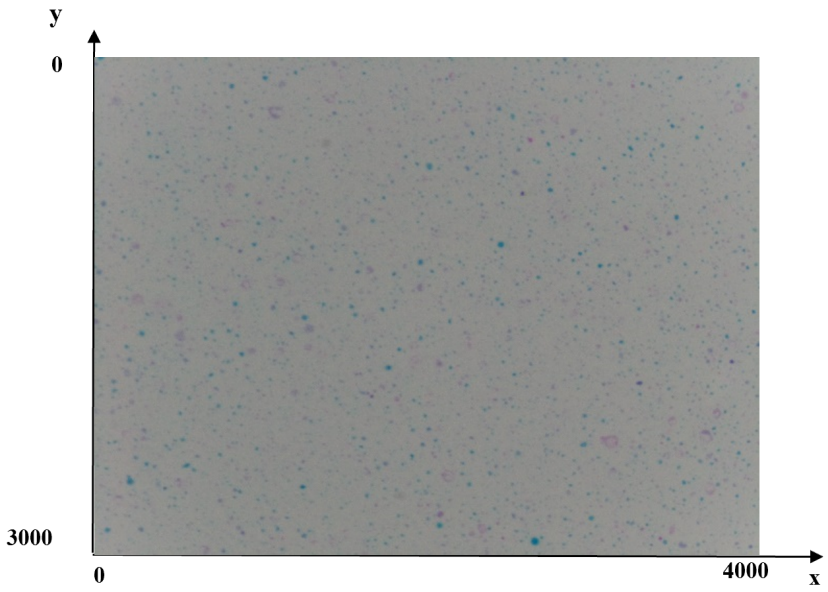

Figure 11. The picture of complex-colour sample taken by the camera system. Both axes in pixels.

Blue blobs. The python processing results of blue droplets in the complex colour sample are shown in the figure (droplets are marked by green circles), the number of droplets is 437, the average diameter is 7.04μm, and the average area is 52.01μm².

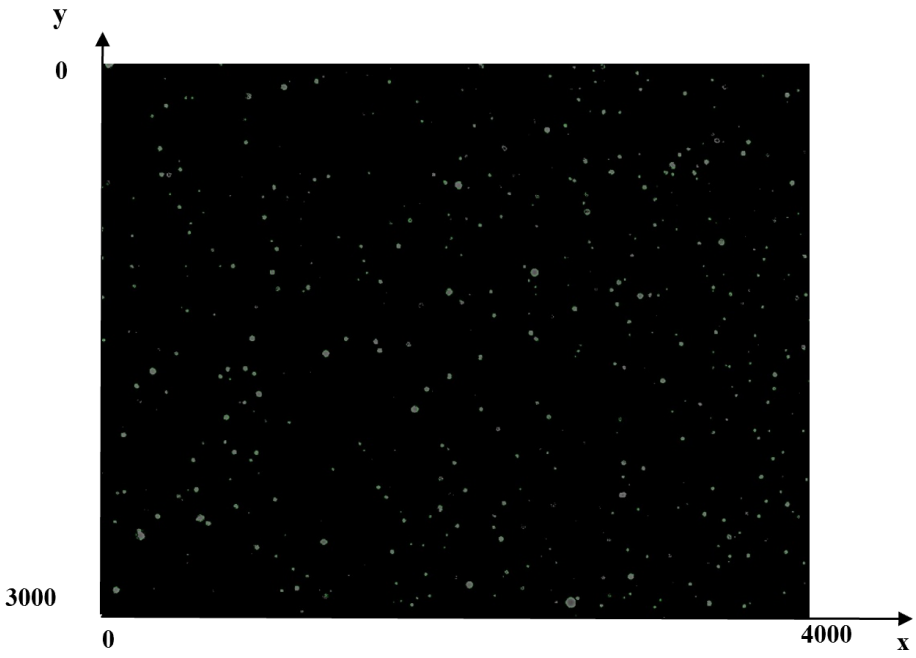

Figure 12. The blue droplets of the complex-colour sample after process of Python.

	Droplet of largest size	Droplet of smallest size

Pixel coordinates	（2687, 2956）	（3519, 873）
Diameter(μm)	27.96	1.83
Area(μm²)	613.97	2.63

Table 5. Data for the largest and smallest blue droplets in the complex-colour sample.

The diameter distribution of blobs is as follows.

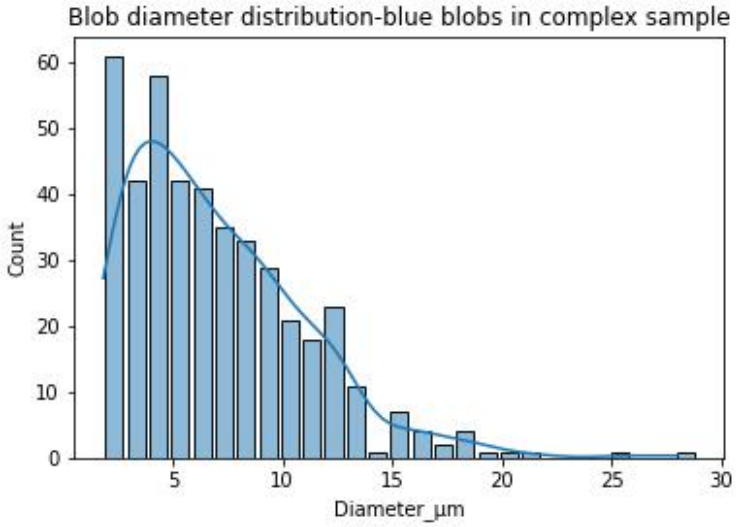

Figure 13. Diameter distribution of the blue droplets in complex-colour sample.

It was shown from the above figure that the two ranges with the largest distribution of spot diameters in the detection area were 1.83 μm–2.83 μm and 3.83 μm–4.83 μm, accounting for 13.96% and 13.27% respectively. The diameters of most of the blobs ranged from 1.83 μm to 10.83 μm, and the quantity accounted for 78.03%.

Droplet concentration	**Value**
Droplet area concentration (%) Total droplet area / detection area	（437×52.01）/（3×10^6）=0.76%
Quantity concentration (particles/mm²) Quantity of droplets / detection area	437/3=146

Table 6. Concentration of the blue droplets in the complex-colour sample.

Pink blobs. The python processing results of pink droplets in the complex colour sample are shown in the figure (droplets are marked by green circles), the number of droplets is 353, the average diameter is 5.18μm, and the average area is 30.00μm².

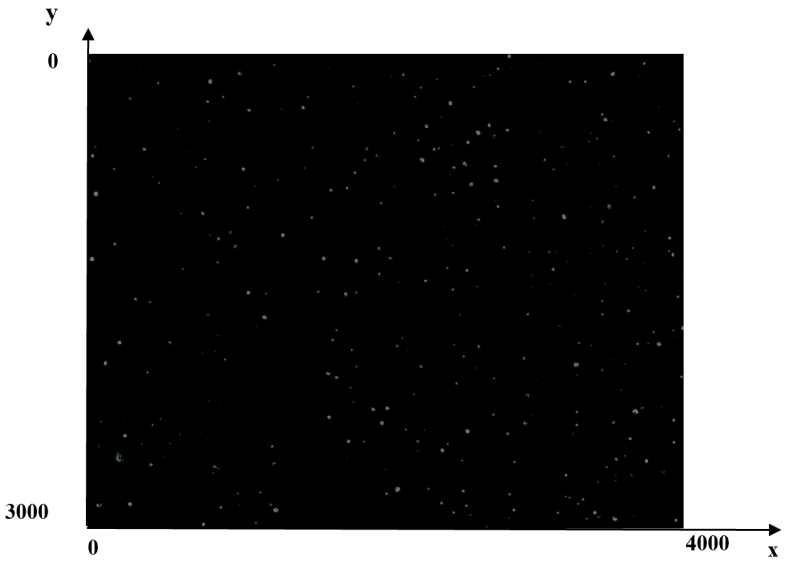

Figure 14. The pink droplets of the complex-colour sample after process of Python.

	Droplet of largest size	Droplet of smallest size
Pixel coordinates	（222, 2592）	（390, 617）
Diameter(μm)	19.69	1.25
Area(μm²)	304.45	1.23

The diameter distribution of blobs is as follows

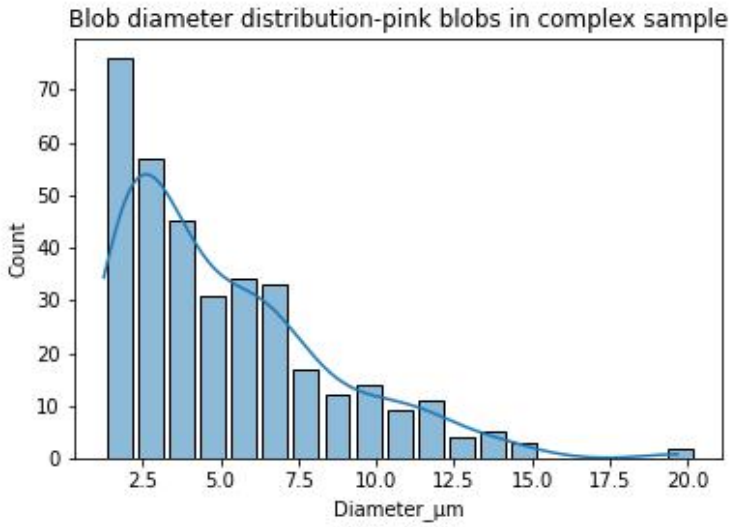

Figure 15. Diameter distribution of the pink droplets in complex-colour sample.

It is shown from the above figure that the largest distribution of spot diameters in the detection area is 1.25μm-2.25μm, accounting for 21.53% of the total. The diameters of most of the spots ranged from 1.25 μm to 8.25 μm, and the quantity accounted for 78.19%.

Table 7 Concentration of the pink droplets in the complex-colour sample.

Droplet concentration	Value
Droplet area concentration (%) Total droplet area / detection area	（353×30）/（3×10^6）=0.35%
Quantity concentration (particles/mm²) Quantity of droplets / detection area	353/3=118

Therefore, in the complex-colour sample, the blue and pink droplets could be well distinguished by the detection system.

For the blue droplets, the total quantity was 437. The diameter range of droplets was from 1.83 to 27.96μm. 78.03% of droplets were at the range of 1.83 μm to 10.83 μm. The area concentration and quantity concentration of the droplets were 0.76% and 146 / mm² respectively.

For the pink droplets, the total quantity was 353. The diameter range of the droplets was from 1.25 to 19.69μm. 78.19% of droplets were at the range of 1.25 μm to 8.25 μm. The area concentration and quantity concentration of the droplets were 0.35% and 118 / mm² respectively.

Photographing and detection of fluorescent samples

Fluorescent droplets. The image below is a picture of the 7-(Diethylamino)-coumarin-3-carboxylic acid sample under UV light, which showed only a few tiny fluorescence spots.

Figure 16. Picture of the fluorescent droplets taken by the camera system.

Under similar sampling conditions, the observability of this sample was far worse than the previously mentioned visible-light-absorbing sample, which was due to the difference in solvent. According to the research of C.E.Ejim et al. (15), under the same air flow, the particle size of atomized particles will be affected by solution viscosity and surface tension, and the increase of solution viscosity or surface tension will increase the size of atomized particles. DMF has a

viscosity of 0.802 mPa·s and a surface tension of 25.7 dyne/cm, while water has a viscosity of 2.98 mPa·s and a surface tension of 72.8 mN/m. The viscosity and surface tension of DMF are both smaller than those of water, which will cause the particle size of the DMF solution to be much smaller than that of the aqueous solution during atomization. Therefore, the 7-(Diethylamino)-coumarin-3-carboxylic acid sample has an observability much worse than that of aqueous samples.

The python processing result of this sample is shown in the figure (droplets are marked by green circles), the number of droplets is 155, and the average area is 8.86μm². Since the droplets in this sample were irregular in shape, this project only used the droplet area to indicates its size.

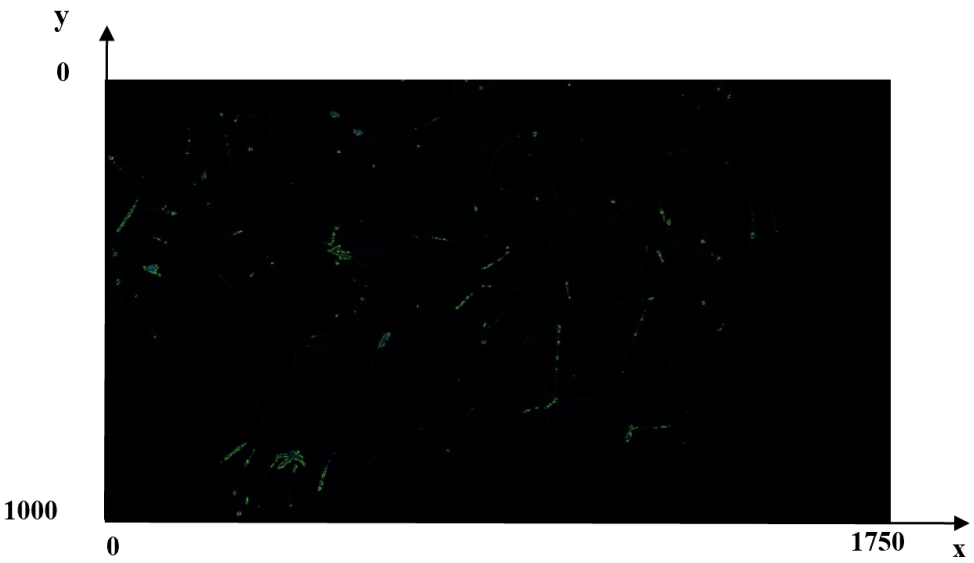

Figure 17. Image of Figure 24 processed using OpenCV.

	Droplet of largest size	**Droplet of smallest size**
Pixel coordinates	（453,922）	（352,925）
Area(μm²)	243.50	0.13

Table 8 Data for the largest and smallest fluorescent droplets.

The distribution of spot area is as follows:

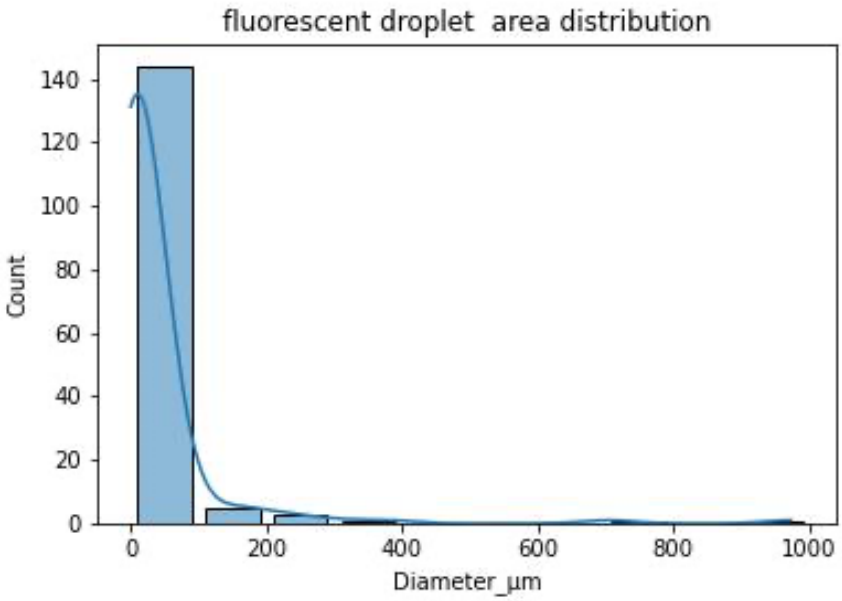

Figure 18. Area distribution of the fluorescent droplets.

Most of the spot areas in the detection area were concentrated in 0.13μm²-20.13μm², accounting for 92.90%, which also verified the research of C.E.Ejim et al. (15), that the size of the atomized particles would vary with the surface tension or viscosity of the solution.

Droplet concentration	Value
Droplet area concentration (%) Total droplet area / detection area	（155×8.86）/（3×10^6）=0.05%
Quantity concentration (particles/mm²) Quantity of droplets / detection area	155/3=52

Table 9. Concentration of the fluorescent droplets.

Therefore, in the fluorescent droplet sample, the total quantity was 155. The area range of droplets was from 0.13 to 243.50μm². 92.90% of droplets were at the range of 0.13μm²-20.13μm². The area concentration and quantity concentration of the droplets were 0.05% and 52 / mm² respectively.

Fluorescent powder. Since the size of the fluorescent droplets in the previous section was too small, the observability of the sample photos was not sufficient, so this project added an experiment to detect the dispersed fluorescent dye (6,7-Dihydroxycoumarin-3-carboxylic acid) powder directly. The Raspberry Pi camera takes pictures as follows:

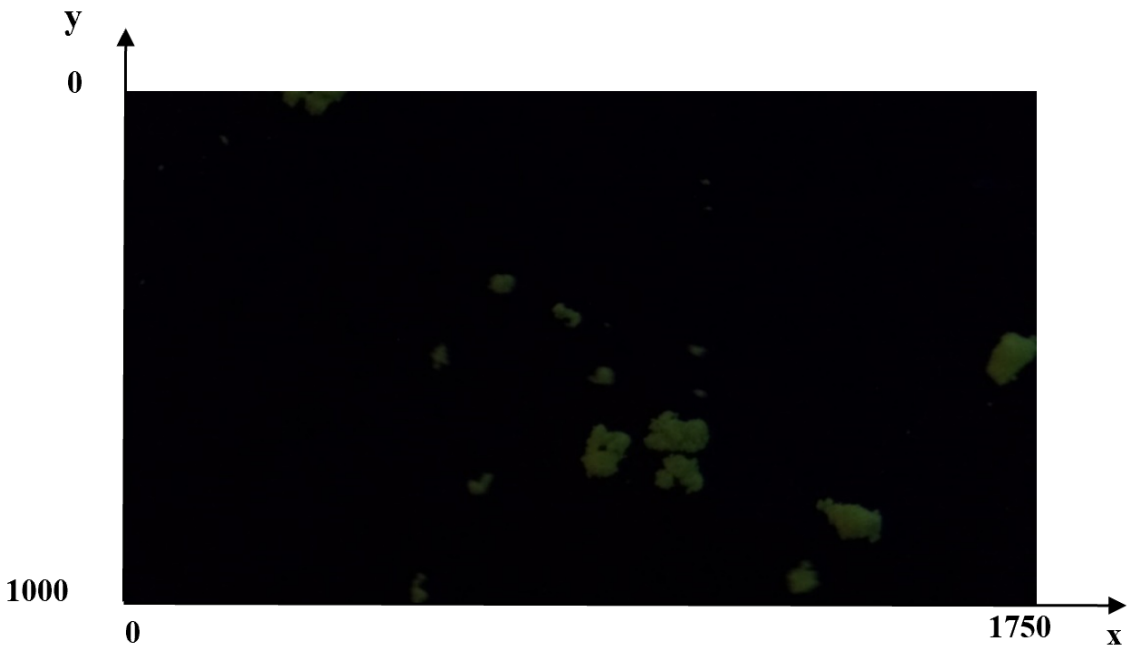

Figure 19. Picture of the fluorescent powder taken by the camera system.

The python processing result of this sample was shown in the figure (the powder is marked with a green circle), and the actual number of powders is 60, but because there are powders with too large area (more than 500μm²) in the observed area, these powders are ignored in the calculation process in this project , so the number of powders is 53 and the average area is 31.86 μm², which, as expected, is larger than the average size of the fluorescent droplets.

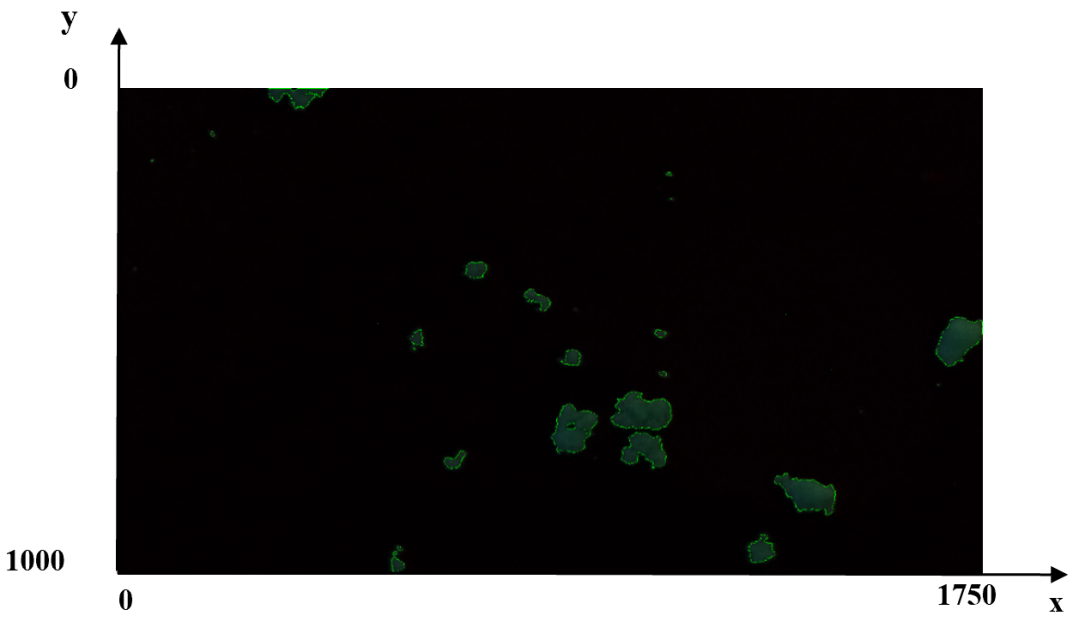

Figure 20. Image of Figure 27 processed using OpenCV. Both axes in pixels.

	Powder of largest size	Powder of smallest size

Pixel coordinates	（795,402）	（576,522）
Area(μm²)	323.88	0.25

Table 10. Data for the largest and smallest fluorescent powder.

The area distribution of powder is as follows:

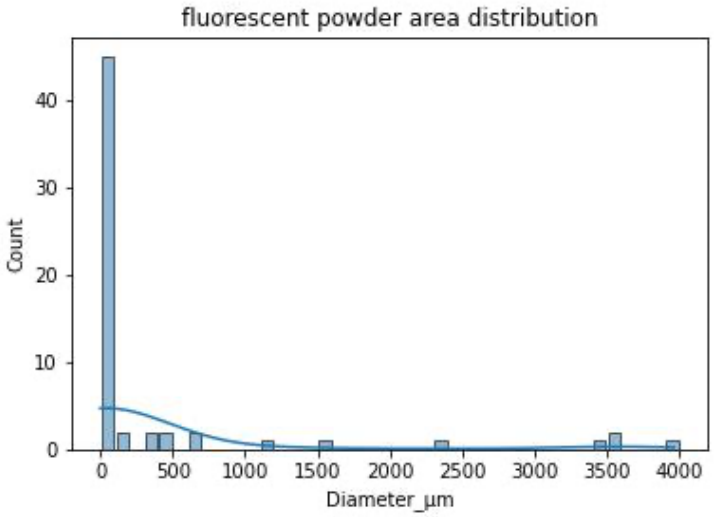

Figure 21. Area distribution of the fluorescent powder.

Most of the spot areas in the detection area are concentrated in 0.25μm²-25.25μm², accounting for 83.02%.

Powder concentration	Value
Powder concentration (%) Total droplet area / detection area	（53×31.86）/（3×10^6）=0.06%
Quantity concentration (particles/mm²) Quantity of droplets / detection area	53/3=18

Table 11. Concentration of the fluorescent powder.

Therefore, in the fluorescent powder sample, the total quantity was 53. The area range of droplets was from 0.25 to 323.88μm². 83.02% of droplets were at the range of 0.25μm²-25.25μm². The area concentration and quantity concentration of the droplets were 0.06% and 18 / mm² respectively.

Accuracy validation of the detection system

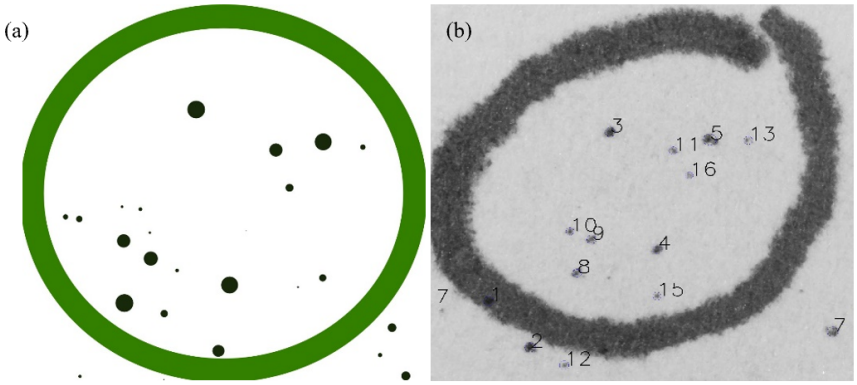

Figure 22. (a) The designed detection area with spots of known size. (b) The image obtained through the detection system.

Considering the limited performance of laboratory printers, which could not print particularly small spots, so when drawing spots in the Inkscape software, the size of the spots was appropriately increased, ranging from tens of microns to 200 microns. Comparing Inkscape's drawing with the actual printed area, it was found that the printing performance was as expected: those spots with a diameter of less than 59 μm were not printed, and there were 10 detectable spots in the selected area. Besides, due to the huge difference between the actual size and the set size of the 13th spot, it was ignored in the calculation process. Meanwhile, due to the limitation of the printer performance, the calculation of quantity error is of little significance, so it was also ignored in this section. The coordinates and size information of the remaining points are shown in the table below.

	Coordinate		Diameter (μm)			Area (μm²)		
Spot #	**x**	**y**	**Measured**	**Set**	**Error**	**Measured**	**Set**	**Error**
3	1615	1032	143	197	-27%	16121	30465	-47%
4	1957	1978	141	189	-25%	15791	28040	-44%
5	2333	1091	185	189	-2%	26943	28040	-4%
8	1378	2169	126	199	-37%	12479	31086	-60%
9	1481	1897	136	158	-14%	14593	19596	-26%
10	1326	1832	116	149	-22%	10685	17427	-39%
11	2069	1181	117	146	-19%	10855	16733	-35%
15	1953	2354	121	131	-7%	11563	13471	-14%
16	2185	1381	107	89	21%	9080	6217	46%
Average					**-15%**			**-24%**

Table 12. Data for the spots in the validation section.

After processing the data, it was calculated that the average measurement error of the detection method for diameter is -15%, and the average measurement error for area is -25%. There is a relationship between diameter and area: area=(π×diameter²)/4, so the error values of the two are

similar, and the two errors are acceptable.

In addition, it should be noted that the test error in this project is mainly affected by three factors: the printing resolution of the printer, the quality of the printing ink/paper and the parameter settings of the blob filter in the Python code.

a. In addition to the loss of small-sized spots, the low print resolution may also result in the loss of edges of large-sized spots, resulting in the circular area captured using OpenCV being smaller than the set size.
b. Poor quality printing ink/paper could cause spreading or condensation of the ink on the paper, which can also affect measurement of spot size.
c. The parameter setting of the blob filter in Python is an unavoidable error, and it is necessary to debug the detector parameters many times to obtain the parameters with the smallest error.

Combined with the analysis of the factors affecting the error, this paper believes that the validation method needs to be further improved. In order to avoid the influence of the printer performance and printing ink/paper on the detection, other substances can be considered to replace the printed spots, such as the commercial Polystyrene Microspheres of known size (16). Since the detection system designed in this project could detect particles at the sub-micron level, the polystyrene microspheres with a size of 1 μm could be detected by the detection system and thus a more accurate measurement error could be calculated. This paper predicts that if the second validation method is adopted, the influence of the printer and printing ink/paper on the detection will be avoided, resulting in the final error much smaller than that of the printing validation method, and further prove the accuracy of the detection system designed in this project is feasible and accurate.

Conclusion

This project designed a chemical particle detection system based on Raspberry Pi camera and Zoom-stereomicroscope. The system was divided into camera system (Raspberry Pi, Raspberry Pi camera module and Zoom-stereomicroscope) and detection system (python code based on openCV function).

In this project, four samples with different light absorption properties were photographed and detected. The experimental results showed that the outline and colour of the droplets could be clearly observed on the sample pictures with the naked eye, proving the excellent imaging performance of the system. Meanwhile, the Python code was used to detect the image, and the minimum diameter of the circular droplet was 1.25μm, and the minimum area of the irregular-shaped droplet was 0.13μm², which proved that the system could detect the quantity and size of micron and submicron particles, as well as the distinguishment of complex-colour samples. Finally, with the validation method of spot drawing-printing-detection, it was calculated that the diameter detection error of the system is -15%, and the area detection error is -25%, both of which were within the acceptable range, which proved the system could detect particles with high accuracy.

What needs to be added is that this report believes that the validation section of this project needs

to be further refined. The validation method based on spot drawing-print-detection adopted in this project was affected by the performance of the printer and the quality of printing ink/paper, which would cause certain errors. In order to eliminate this error, it is believed that commercial polystyrene microspheres of known size can be detected to get a more accurate detection error by comparing the detection results with the product specifications. In addition, this paper believes that in addition to detecting micron/submicron particles on the solid surface, the detection system can also realize the detection of nanoparticles by selecting commodity digital cameras with higher imaging performance, or by rewriting the python code to realize the real-time monitoring of chemical particles in fluids.

In recent years, most mobile phone manufacturers have vigorously developed and promoted the camera performance of mobile phones, so this paper believes that the camera performance of commodity digital cameras will be rapidly improved in the future. At the same time, the rapid detection technology of chemical particles based on commodity digital cameras will have a greater potential for application, and more researchers are needed to invest in this field.

Acknowledgements

This work was generously supported by the Leverhulme Trust (Early Career Fellowship ECF-2021-298).

Bibliography

(1) Benning, J. L., Liu, Z., Tiwari, A., Little, J. C., & Marr, L. C. (2013). Characterizing Gas-Particle Interactions of Phthalate Plasticizer Emitted from Vinyl Flooring. Environmental Science & Technology, 47(6), 2696–2703. https://doi.org/10.1021/es304725b

(2) Eriksson, A. C., Andersen, C., Krais, A. M., Nøjgaard, J. K., Clausen, P.-A., Gudmundsson, A., Wierzbicka, A., & Pagels, J. (2020). Influence of Airborne Particles' Chemical Composition on SVOC Uptake from PVC Flooring—Time-Resolved Analysis with Aerosol Mass Spectrometry. Environmental Science & Technology, 54(1), 85–91. https://doi.org/10.1021/acs.est.9b04159

(3) Prajitha, N., Athira, S. S., & Mohanan, P. V. (2019). Bio-interactions and risks of engineered nanoparticles. Environmental Research, 172, 98–108. https://doi.org/10.1016/j.envres.2019.02.003

(4) You, C.-C., Miranda, O. R., Gider, B., Ghosh, P. S., Kim, I.-B., Erdogan, B., Krovi, S. A., Bunz, U. H. F., & Rotello, V. M. (2007). Detection and identification of proteins using nanoparticle–fluorescent polymer 'chemical nose' sensors. Nature Nanotechnology, 2(5), 318–323. https://doi.org/10.1038/nnano.2007.99

(5) Zhu, Y. Y., Ding, G. Q., Ding, J. N., & Yuan, N. Y. (2010). AFM, SEM and TEM Studies on Porous Anodic Alumina. Nanoscale Research Letters, 5(4), 725–734. https://doi.org/10.1007/s11671-010-9538-9

(6) Bogoch, I. I., Koydemir, H. C., Tseng, D., Ephraim, R. K. D., Duah, E., Tee, J., Andrews, J. R., & Ozcan, A. (2017). Evaluation of a Mobile Phone-Based Microscope for Screening of Schistosoma haematobium Infection in Rural Ghana. The American Journal of Tropical Medicine and Hygiene, 96(6), 1468–1471. https://doi.org/10.4269/ajtmh.16-0912

(7) Wei, Q., Qi, H., Luo, W., Tseng, D., Ki, S. J., Wan, Z., Göröcs, Z., Bentolila, L. A., Wu, T.-T., Sun, R., & Ozcan, A. (2013). Fluorescent Imaging of Single Nanoparticles and Viruses on a Smart Phone. ACS Nano, 7(10), 9147–9155. https://doi.org/10.1021/nn4037706

(8) Zhang, Z., Wang, H., Su, M., Sun, Y., Tan, S., Ponkratova, E., Zhao, M., Wu, D., Wang, K., Pan, Q., Chen, B., Zuev, D., & Song, Y. (2021). Printed Nanochain-Based Colorimetric Assay for Quantitative Virus Detection. Angewandte Chemie International Edition, 60(45), 24234–24240. https://doi.org/10.1002/anie.202109985

(9) Yan, C., Chunyan, M., Zaihe, S., & Rui, C. (2019). Research on Vibration Characteristics of Piezoelectric Ceramic Atomizer Based on ANSYS. E3S Web of Conferences, 118, 02043. https://doi.org/10.1051/e3sconf/201911802043

(10) Cao, Li, Zhang, Xuemei, Hu, Gang, & Huang, Fangfang. (n.d.). Microporous Atomization Plate (Patent No. 20210053085).

(11) Wang, R., Guan, S., Sato, A., Wang, X., Wang, Z., Yang, R., Hsiao, B. S., & Chu, B. (2013). Nanofibrous microfiltration membranes capable of removing bacteria, viruses and heavy metal ions. Journal of Membrane Science, 446, 376–382. https://doi.org/10.1016/j.memsci.2013.06.020

(12) Hong, Y., Lam, J. W. Y., & Tang, B. Z. (2009). Aggregation-induced emission: phenomenon, mechanism and applications. Chemical Communications, 29, 4332–4353. https://doi.org/10.1039/B904665H

(13) Luo, J., Xie, Z., Lam, J. W. Y., Cheng, L., Chen, H., Qiu, C., Kwok, H. S., Zhan, X., Liu, Y., Zhu, D., & Tang, B. Z. (2001). Aggregation-induced emission of 1-methyl-1,2,3,4,5-pentaphenylsilole. Chemical Communications, 18, 1740–1741. https://doi.org/10.1039/B105159H

(14) Hu, Y., Chen, Q., Tao, T., Li, H., & Zuo, C. (2017). Absolute three-dimensional micro surface profile measurement based on a Greenough-type stereomicroscope. Measurement Science and Technology, 28(4), 045004. https://doi.org/10.1088/1361-6501/aa5a2d

(15) Ejim, C. E., Rahman, M. A., Amirfazli, A., & Fleck, B. A. (2010). Effects of liquid viscosity and surface tension on atomization in two-phase, gas/liquid fluid coker nozzles. Fuel, 89(8), 1872–1882. https://doi.org/10.1016/j.fuel.2010.03.005

(16) Kuriyama, A., & Ozaki, Y. (2014). Assessment of Active Pharmaceutical Ingredient Particle Size in Tablets by Raman Chemical Imaging Validated using Polystyrene Microsphere Size Standards. AAPS PharmSciTech, 15(2), 375–387. https://doi.org/10.1208/s12249-013-0064-9